DOI 10.1007/s11182-021-02432-0
Russian Physics Journal, Vol. 64, No. 6, October, 2021 (Russian Original No. 6, June, 2021)

INFLUENCE OF GEOMETRIC TOOTH SHAPE PARAMETERS OF LABYRINTH SEALS ON THE FLOW LAW AND THE ALGORITHM FOR DESIGNING STRAIGHT GRATE TEETH

Bo Zhang,[1] Jingjing Li,[1] Wenkai Li,[2] and Honghu Ji[1]

UDC 533.08

In view of the fact that the traditional method does not summarize flow rules through straight labyrinth seals, there is no rule to summarize the sealing effects of the labyrinth seals with different specifications. Therefore, it is proposed to study the influence of the geometric tooth profile parameters on the flow law and the algorithm for designing the labyrinth seals. According to the geometric tooth profile parameters, 22 tooth profile test models of straight tooth grating have been designed. Experimental results have shown that the flow coefficient increases with the seal clearance and the tooth tip thickness. It is proportional to the tooth height, pitch, and the number of teeth. When compressed air passes through the labyrinth seals, to improve the sealing effect, attention should be focused on the design of the first and last teeth. This provides a favorable basis for the study of the flow law in the labyrinth.

Keywords: straight-through labyrinth seals, geometric parameters, sensitivity grade, discharge coefficient.

INTRODUCTION

Nowadays the high temperature and pressure ratio in a steam and gas turbine engine leads to poor sealing between the stator and the fixed parts of the engine. The performance of the engine is closely related to the fuel ratio, and the less the leakage rate, the stronger is the engine [1–3]. Therefore, reducing the leakage is the most important step in achieving high performance characteristics of the grate seal. Grate seal is very important for the turbine design because the turbine performance is closely related to the quality of the grate seal and its cost is low. The grate seal fluidity refers to the flow of a series of high friction paths restricted bypass. The total sealing outlet pressure is closely related to the loss of individual restrictions, and the limiting loss will reduce the export pressure. As the flow passes through the grate seal, the pressure decreases with increasing seal length. The cause of the local static pressure is a sudden expansion of a stagnation point, fluid in and out in different sealing space [4, 5].

The design of the grate seal is more complex, the pressure ratio of the seal and the engine speed will affect the emission characteristics [6–9]. Yang *et al*. [10] studied the leakage characteristics of the grate seal for different values of pressure ratios and radial clearances. The blade thickness and the blade profile of the steam turbine were studied using a static test bench, and a relationship between the eccentricity and the geometric parameters was discussed, but the rules were not summarized. Cui *et al*. [11] analyzed a relationship between the leakage flow rate of the labyrinth seal and the cavity pressure for different combinations of the pressure ratio and the rotational speed and carried out measurements and numerical simulations. However, they did not study the labyrinth seals for tightness. Fu *et al*. [12] studied the effect of tooth spacing, shaft diameter, Reynolds number, and gap on the residual coefficient, but provided

[1]Jiangsu Province Key Laboratory of Aerospace Power System, College of Energy and Power, Nanjing University of Aeronautics and Astronautics, Nanjing, China, e-mail: zhangbo_pe@nuaa.edu.cn; 15950500096@163.com; NUAA0096dyy@163.com; [2]Jiangsu Key Laboratory of Green Process Equipment, Changzhou, China, e-mail: hq229818631@163.com. Translated from Izvestiya Vysshikh Uchebnykh Zavedenii, Fizika, No. 6, pp. 138–144, June, 2021. Original article submitted November 24, 2020.

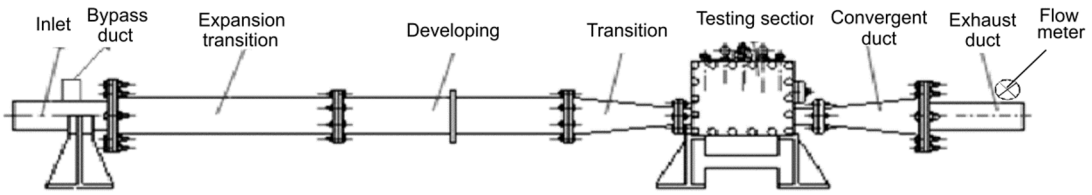

Fig. 1. Sketch of the experimental rig.

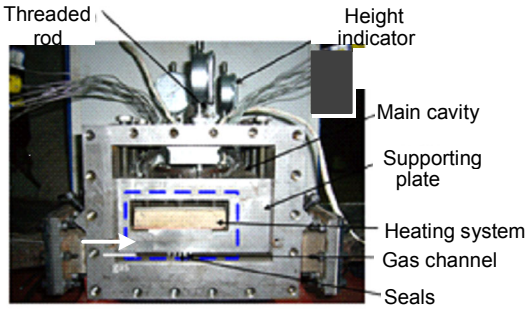

Fig. 2. Labyrinth seal section.

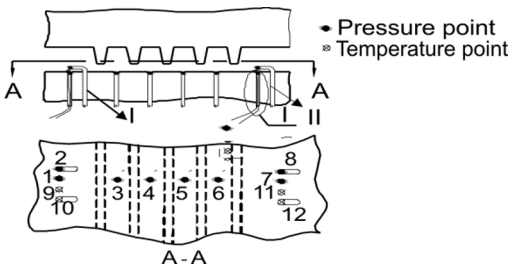

Fig. 3. Sketch of the labyrinth seal.

no regular summary. Zhang *et al*. [13] studied the leakage of the maze combined with the theory and compared the results obtained. However, the designed algorithm was not perfect, it still had sealing defects. To explain the relationship between the variables and targets, the method of dimensionless interdependent analysis was proposed by Cui *et al*. [14] and Wang *et al*. [15]. However, this method did not summarize the straight grate tooth flow patterns. Yang *et al*. [16] studied numerical results for some geometric arrangements in which the leakage flow was mixed with the main flow in different ways; however, this method still had the problem with gear arrangement.

With allowance for the foregoing, this paper is devoted to the study of the influence of the geometric tooth profile parameters on the flow law and the algorithm for designing the labyrinth seals. Summarizing the flow rule through the straight teeth under the influence of the geometric parameters, 22 test models of the straight labyrinth teeth with different tooth height, spacing, tip thickness, and number were designed. Experiments were carried out with different models to test the leakage flow through a linear labyrinth seal. In this paper, the influence of different parameters on the sealing flow is studied, and the sequence of sealing leakage effects is discussed. It is of scientific significance to summarize the flow rules through the labyrinth seals and to study their algorithmic implementation.

MATERIALS AND METHODS

To summarize the flow pattern through the labyrinth seals, experimental materials and methods were used. Figure 1 shows a static test device. As can be seen from Fig. 1, a gas flows into a closed test vessel under the action of the expansion tube and then flows out from the exhaust pipe [17]. The inlet width of the test vessel was 200 mm and its height was 12 mm, while the width of the outlet was 200 mm and the width was reduced to 10 mm. During our experiment, the closed model was kept stationary on a supporting plate (Fig. 2), and the widths of all models were the same and equal to 200 mm (Fig. 2). The gas flowed out through the common channel below the supporting plate and the main cavity (as indicated by the arrow) described by three non-collinear points used to adjust the flow height in order that three heights remained unchanged from the data of indicators of the same types to ensure that the channel is oriented horizontally. Figure 3 shows the heating system in more detail (the instrument panel is shown in Fig. 2) with the thermocouples placed horizontally below the channel. Their locations are shown by dots in Fig. 3. Figure 4 shows

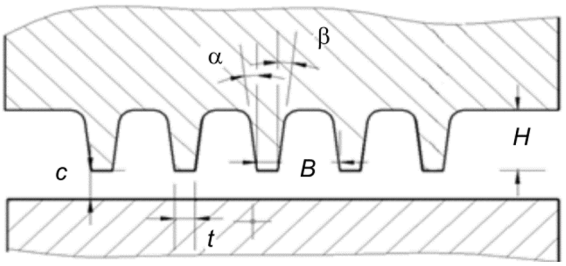

Fig. 4. Labyrinth seal parameters.

distributions of the temperature and pressure pilots. The hydrostatic guides are placed between epy neighboring teeth, and the total pressure guides are placed at the inlet (indicated by I) and outlet (indicated by II). The experiment was carried out at a pressure ratio increasing from 1.2 to 1.8. Figure 3 shows the model of the labyrinth seal space, and Fig. 4 shows the pressure distribution at measurement points. The pressure through the drinking water pipe was measured at the seal entrance.

LABYRINTH SEAL DESIGNS

The labyrinth seal was designed using the materials and methods described above. Figure 4 shows dimensions of the straight-through grate seal space. The main geometric parameters were the tooth tip thickness *t*, the sealing clearance C, the sealing height H, the sealing joint B, the front seal cone angle α, and the rear seal cone angle β. The geometric parameters changed in the following ranges: $0.1\ \text{mm} \le c \le 0.7\ \text{mm}$, $0.2\ \text{mm} \le t \le 0.6\ \text{mm}$, $3\ \text{mm} \le H \le 7\ \text{mm}$, $3\ \text{mm} \le B \le 9\ \text{mm}$, $0° \le \alpha \le 15°$, and $0° \le \beta \le 15°$. The factor rotation method was used as the main criterion for the experiment with 22 models, and model 3 was regarded as the reference model. The model parameters are presented in Table 1.

Models 1–5 have tooth tip thicknesses t, models 6–9 have sealing heights H, models 10–14 have sealing cavity joints B, models 15–17 have tooth numbers N, and model 18–22 have labyrinth tooth gaps c that differed from those of reference model 3. The front sealing cone angle α and the rare sealing cone angle β were the same as those of model 3. Different seal models are shown in Fig. 5.

EXPERIMENTAL RESULTS AND ANALYSIS

The 22 labyrinth seal models with different specifications discussed above were experimental objects, and the sealing flow rule was the research objective to study the influence of different parameters on the sealing effect. This was provided by the specific standard experimental design. The expressions for the discharge efficiency C_D of the straight tooth seal with a smooth wall were calculated from the following formulas:

$$C_D = \frac{m_r}{m_i}, \tag{1}$$

$$m_i = \frac{p_0 A}{\sqrt{\kappa R T_0}} \sqrt{\frac{2\kappa^2}{\kappa - 1}\left(\frac{p_n}{p_0}\right)^{\frac{2}{\kappa}}\left[1 - \left(\frac{p_n}{p_0}\right)^{\frac{\kappa-1}{\kappa}}\right]}, \tag{2}$$

TABLE 1. Tooth Geometric Parameters

Model No.	*t*, mm	*H*, mm	*B*, mm	*N*	*C*, mm
1	0.2	4.8	4	3	0.3
2	0.3	4.8	4	3	0.3
3	0.4	4.8	4	3	0.3
4	0.5	4.8	4	3	0.3
5	0.6	4.8	4	3	0.3
6	0.4	3	4	3	0.3
7	0.4	4	4	3	0.3
8	0.4	6	4	3	0.3
9	0.4	7	4	3	0.3
10	0.4	4.8	3	3	0.3
11	0.4	4.8	5	3	0.3
12	0.4	4.8	6	3	0.3
13	0.4	4.8	7	3	0.3
14	0.4	4.8	8	3	0.3
15	0.4	4.8	4	2	0.3
16	0.4	4.8	4	4	0.3
17	0.4	4.8	4	5	0.3
18	0.4	4.8	4	3	0.1
19	0.4	4.8	4	3	0.2
20	0.4	4.8	4	3	0.4
21	0.4	4.8	4	3	0.5
22	0.4	4.8	4	3	0.6

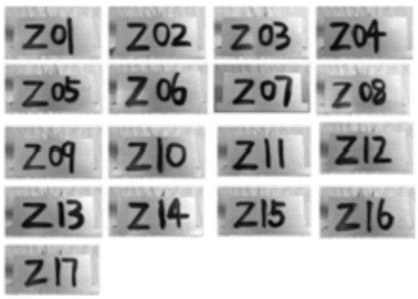

Fig. 5. Different seal models.

where m_r is the leakage mass flow in the flowmeter of the converter and m_i is the theoretical leakage mass flow under the isentropic condition [18]. In the above formula, p_n / p_0 is the ratio of the total inlet and outlet pressures (shown in Fig. 4) that also indicates the pressure along the airway. The area of the spatial gap cross section is $A = W \cdot c$, where W is the labyrinth width and C is the labyrinth tooth gap. The relative variation factor of the discharge efficiency is

$$\varepsilon_i = \frac{ABS(C_{di+1}^{(X)} - C_{di}^{(X)})}{\sum_{i=1}^{n} ABS\left(C_{di+1}^{(X)} - C_{di}^{(X)}\right)} \quad (1 \le i \le n). \tag{3}$$

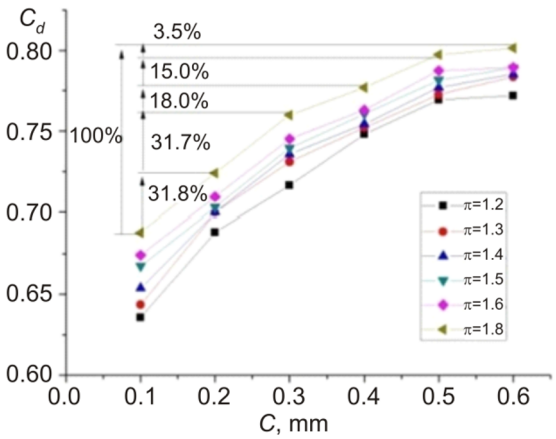

Fig. 6. Flow coefficient versus *C* values.

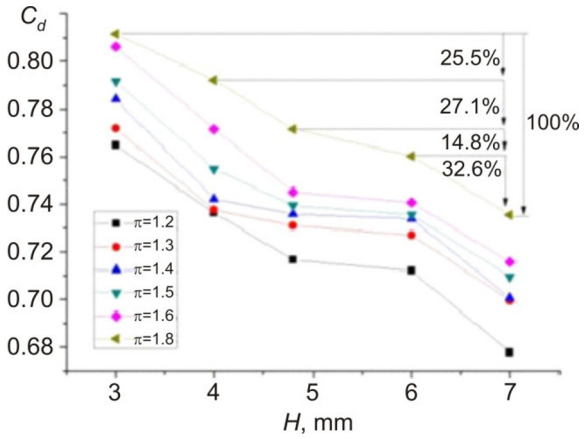

Fig. 7. Flow coefficient versus *H* values.

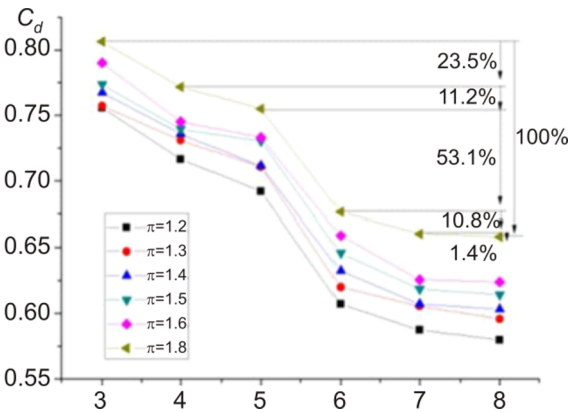

Fig. 8. Flow coefficient versus *B* values.

In the above formula, X is the geometric factor, i denotes the serial number of the geometric factors, and C_d is the discharge efficiency. The calculated results are analyzed for a pressure ratio of 1.6.

To further summarize the sequence of the seal leakage effects, we analyzed the obtained experimental results. Figure 6 shows the relationship between the sealing clearance *c* and the flow coefficient. With continuous expansion of the seal clearance, C_d increases, and the rate of its increase slows down. Taking a pressure ratio of 1.8 as an example, we obtained that the relative variation coefficient decreased with increasing seal clearance [19].

As the seal clearance increased from 0.1 mm to 0.2 mm, the relative variation coefficient ε increased up to 31.8%. When the seal clearance *c* increased from 0.5 to 0.6 mm, the relative variation coefficient ε reduced down to 3.5. In conclusion, when the seal clearance increased, the flow area increased, and the jet velocity at the tooth tip and the swirl velocity in the cavity decreased, thereby leading to the decreased sealing performance [20–25]. With decreasing seal clearance, the leakage performance of the seal also decreased.

Figure 7 shows the relationship between the sealing height *H* and the flow coefficient. With increasing sealing height, the C_d value decreases for each flow coefficient, the cavity volume of the labyrinth seal increases, and the swirl in the cavity monotonically increases, which causes the kinetic energy to dissipate rapidly, thereby reducing the seal leakage.

Figure 8 shows the relationship between the sealing distance *B* and the flow coefficient. When the sealing distance increased from 3 to 4 mm, the factor ε increases up to 23.5%, then to 53.1%, and then to 1.4%. With increasing sealing distance, the cavity volume of the labyrinth seal also increased, the swirl flow in the cavity

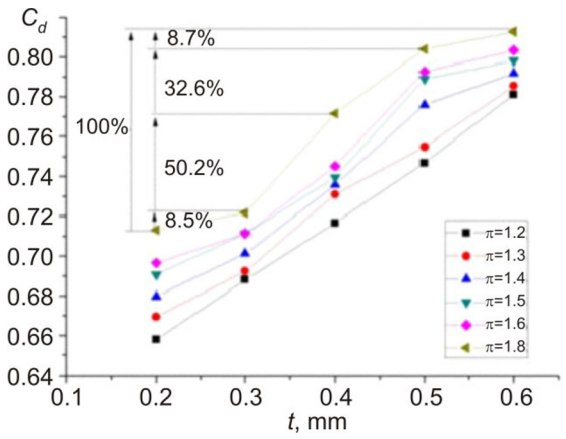

Fig. 9. Flow coefficient versus *T* values.

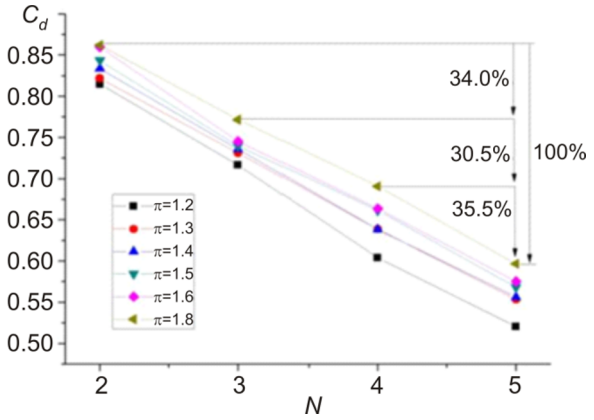

Fig. 10. Flow coefficient versus *N* values.

strengthened, the kinetic energy dissipated rapidly, the dissipative cavity vibration became small, and the C_d value smoothly decreased. The relationship between the head width *t* and the flow coefficient can be seen in Fig. 9. As the head width increases, so does the C_d value. The penetration effect increased, the number of jets flowing down the wall to the tip gap increased, the expansion angle of the jet decreased, the penetration effect increased, and the airtight leakage increased.

Figure 10 shows the relationship between the number of seals and the flow coefficient. With increasing number of seals [26–28], the C_d value decreases, whereas the ε value remains unchanged. With increasing sealing number, the throttling effect of the tooth tip is enhanced, and the swirl in the cavity is enhanced, thereby accelerating the dissipation of the kinetic energy.

During our experiment, the reason for the change of the same flow coefficient was that the geometric parameters were different together with their different range of changes. Therefore, the sensitivity of the geometric parameters to the flow coefficient was analyzed together with the flow sensitivity coefficient. The flow sensitivity coefficient is given by the formula

$$M_X = \frac{\sum_{i=1}^{n} \mathrm{ABS}\left(C_{di+1}{}^{(X)} - C_{di}{}^{(X)}\right)}{X_n - X_1} \quad (1 \le i \le n). \tag{4}$$

Based on the experimental data presented above and formula (5), the sensitivity coefficient of different factors can be estimated. For $\pi = 1.8$, we obtained $MC = 0.2724$, $MT = 0.2488$, $MH = 0.0190$, and $MB = 0.0296$, from which it follows that $MC > MT > MB > MH$, that is, the sequence of the effective change of the unit is $c \to t \to B \to H$. Comparing all the coefficients, we obtain that the trends of change were the same. To sum up, the degree of influence of the trends in changing the parameters on the sensitivity is described by the formula $c \to t \to B \to H$ under the same conditions.

DISCUSSION

Figure 11 shows distributions of the static pressure in the inlet and outlet sections and inside of each labyrinth seal cavity for $N = 2, 3, 4$ separately. As can be seen, the pressure along the axis decreases continuously; moreover, the pressure drop after passage of each cavity of the tooth is almost the same, showing little changes of different pressure ratios.

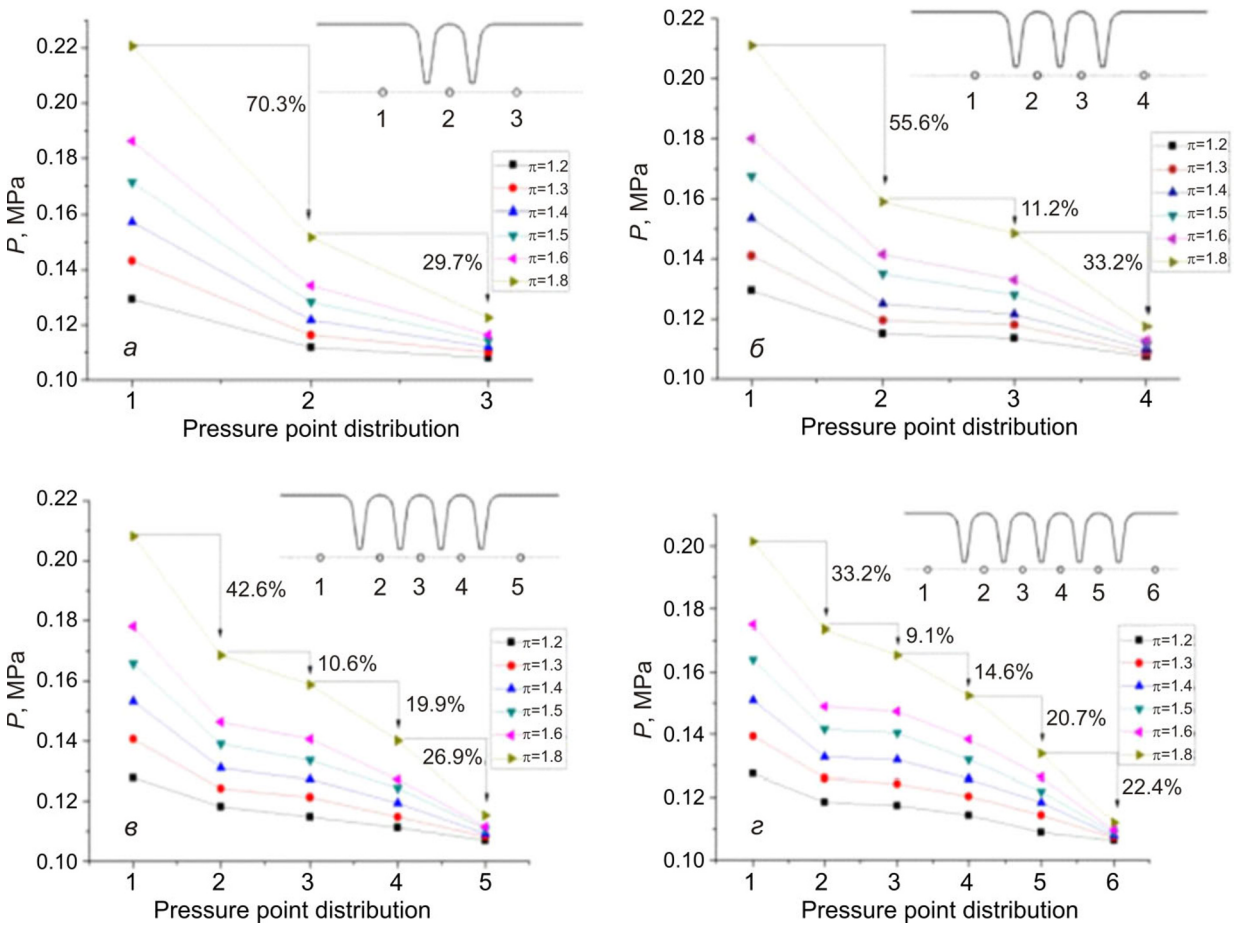

Fig. 11. Pressure variation in the cavity with $N = 2$ (*a*), 3 (*b*), 4 (*c*), and 5 (*d*).

The percentage of the total airflow pressure drop after passage of each tooth of the labyrinth for π=1.8 is shown in Fig. 11. It can be seen that the largest pressure drop occurs after passage of the first and the last teeth. This was caused by the sudden contraction and extension of the flow area [29, 30]. When the air flow entered the first tooth section from the horizontal channel with a sudden contraction section, the air flow is compressed at the tip of the tooth, then it flowed to the first cavity where the throttle area ratio and the jet angle changed strongly, and the pressure dropped suddenly; the same was repeatedly observed for the next tooth. As the tooth number increased from 2 to 5, the proportion of the pressure drop in the first and the last sections gradually decreased. While passing through several middle teeth, the corresponding pressure drop increased to some extent. Moreover, the proportion of the pressure drop in the first section decreased from 70.3% to 33.2%, while it decreased from 29.7% to 22.4% in the last section [31–33]. As can be seen, the first and the last teeth play major roles in the design, and designers should focus on them in the process of labyrinth design. The middle teeth caused relatively small pressure drop with small changes of the areas.

CONCLUSIONS

In this paper, 22 straight labyrinth seals with different geometric parameters have been designed, and the leakage characteristics of the seals have been studied as functions of the tooth tip thickness t, width B, clearance c, height H, and number N for a pressure ratio of 1.2 n. The following results were obtained.

1. In the grate seal, the discharge efficiency increases with the seal pressure ratio, gap c as well as with the tooth height and spacing and the number of teeth.

2. The sequence in which the range of geometric parameters affects the sensitivity of the flow coefficient is $c \to t \to B \to H$.

3. In the labyrinth seal, the first and the last teeth play different roles. With increase in N from 2 to 5, the proportion of the pressure drop in the first section decreased from 70.3% to 33.2%, whereas in the last section it decreased from 29.7% to 22.4%.

As has been demonstrated in this paper, the flow law of the labyrinth seals is well summarized. According to the experiment, when the compressed air passes through the labyrinth seals, the percentage of the pressure drop in the first and last teeth is larger than in the middle teeth. Therefore, attention should be focused on the design of the first and last teeth to improve the sealing effect. This provides a favorable basis for elucidation of the flow law of the labyrinth seals. The application of the labyrinth seals will be the subject of our future research.

This research was funded by National Science and Technology Major Project (2017-1-0001-0001).

REFERENCES

1. R. S. Zhu, Y. G. Lu, *et al*., At. Energy Sci. Tech., **50**, No. 7, 1216–1223 (2016).
2. H. L. Qiao, J. Y. Yu, and C. Wang, J. China Acad. Electron. Inf. Tech., **11**, No. 6, 574–576 (2016).
3. A. Soni and S. N. Singh, Sol. Energy, **148**, 149–156 (2017).
4. T. D. Melo, J. N. V. Goulart, C. T. M. Anflor, *et al*., Eur. J. Mech. B Fluids, **62**, No. 3–4, 130–138 (2017).
5. H. Ye, X. S. Ge, S. Y. Zhuang, *et al*., Acta Energ. Sol. Sin., **24**, No. 1, 27–31(2003).
6. B. Zhang, J. J. Li, W. K. Li, *et al*., J. Comput. Theor. Nanosci., **14**, No. 3, 1528–1534 (2017).
7. M. J. Avanaki, and A. A. A. Jeddi, J. Text. Inst. Proc. Abstr., **108**, No. 3, 418–427 (2016).
8. M. K. Guo, Q. H. Wang, J. Z. Yang, *et al*., J. Yangtze Univ. (Nat. Sci. Ed.), **12**, No. 32, 55–60 (2015).
9. F. Tong, L. Zhang, R. Hua, *et al*., J. Propuls. Tech., **36**, No. 1, 119–123 (2015).
10. Z. H. Yang, H. J. Gong, Y. J. Li, *et al*., China Sciencepaper, **11**, No. 5, 527–532 (2016).
11. L. Cui, G. Q. Li, G. Han, *et al*., Gas Turb. Technol., **30**, No. 1, 41–47 (2017).
12. X. Fu, Y. H. Cao, Y. B. Zhang, *et al*., Acta Armamentarii, **38**, No. 4, 824–832 (2017).
13. B. Zhang, H. H. Ji, F. Q. Du, *et al*., J. Propuls. Technol., **37**, No. 2, 304–310 (2016).
14. H. F. Cui, S. N. Liao, and Q. W. Gao, Intern. Combust. Eng., **34**, No. 6, 1–4 (2016).
15. H. G. Wang, and C. J. Su, J. Netshape Forming Engineering., **25**, No. 1, 66–70 (2017).
16. F. Yang, H. S. Zhu, S. Q. Jiao, *et al*., West-China Explor. Eng., **28**, No. 5, 47–49 (2016).
17. L. Teng, Y. X. Li, M. Liu, *et al*., Oil Gas Storage Transp., **35**, No. 11, 1179–1186 (2016).
18. Z. Lei, X. Z. Kong, G. W. Liu, *et al*., J. Propuls. Technol., **38**, No. 11, 2588–2596 (2017).
19. Z. K. Wang, Z. X Zeng, Y. H. Xu, *et al*., J. Propuls. Technol., **36**, No. 3, 405–412 (2015).
20. F. Wu, K. L. Lu, and Y. Xiao, Fire Sci. Technol., **34**, No. 7, 863–865 (2015).
21. W. Gao, and W. Wang, Colloq. Math., **147**, No. 1, 55–65 (2017).
22. L. Kang, H. L. Du, X. Du, *et al*., Desalin. Water Treat., **4**4, No. 25, 296–301 (2018).
23. D. Li, L. Wang, W. Peng, *et al*., Polymer Compos., **38**, No. 9, 2009–2015 (2017).
24. A. M. Simoes, J. Interdiscip. Math., **21**, No. 3, 645–667 (2018).
25. M. A. Styugin, A. A. Kytmanov, and T. N. Yamskikh, J. Discrete Math. Sci. Cryptogr., **21**, No. 3, 679–694 (2018).
26. W. Gao and W. F. Wang, J. Differ. Equ. Appl., **23**, Nos. 1–2, Special Issue, 100–109 (2017).
27. W. Gao and W. Wang, Colloq. Math., **149**, No. 2, 291–298 (2017).
28. M. I. García-Planas and T. Klymchuk, Appl. Math. Nonlinear Sci., **3**, No. 1, 97–104 (2018).
29. F. Dusunceli, Appl. Math. Nonlinear Sci., **4**, No. 2, 365–370 (2019).
30. W. Zhao, T. Shi, and L. Wang, Appl. Math. Nonlinear Sci., **5**, No. 1, 71–84 (2020).
31. H. Harraga and M. Yebdri, Appl. Math. Nonlinear Sci., **3**, No. 1, 127–150 (2018).
32. A. M. Nasir, S. M. Husnine, T. Ak, *et al*., Math. Meth. Appl. Sci., **41**, No. 16, 6611–6624 (2018).
33. V. Fabian Morales-Delgado, J. Francisco Gomez-Aguilar, and A. Atangana, Therm. Sci., **23**, No. 2B, 1279–1287 (2019).